THE JOURNAL OF PHYSICAL CHEMISTRY LETTERS
A JOURNAL OF THE AMERICAN CHEMICAL SOCIETY

pubs.acs.org/JPCL

Letter

A Mechanoelastic Glimpse on Hyaluronan-Coated Extracellular Vesicles

Debashish Paul,[#] Anirban Paul,[#] Dipanjan Mukherjee,[#] Saroj Saroj, Manorama Ghosal, Suchetan Pal,[*] Dulal Senapati,[*] Jaydeb Chakrabarti,[*] Samir Kumar Pal,[*] and Tatini Rakshit[*]

Cite This: *J. Phys. Chem. Lett.* 2022, 13, 8564−8572

Read Online

ACCESS | Metrics & More | Article Recommendations | Supporting Information

ABSTRACT: Cancer cells secrete extracellular vesicles (EVs) covered with a carbohydrate polymer, hyaluronan (HA), linked to tumor malignancy. Herein, we have unravelled the contour lengths of HA on a single cancer cell-derived EV surface using single-molecule force spectroscopy (SMFS), which divulges the presence of low molecular weight HA (LMW-HA < 200 kDa). We also discovered that these LMW-HA-EVs are significantly more elastic than the normal cell-derived EVs. This intrinsic elasticity of cancer EVs could be directly allied to the LMW-HA abundance and associated labile water network on EV surface as revealed by correlative SMFS, hydration dynamics with fluorescence spectroscopy, and molecular dynamics simulations. This method emerges as a molecular biosensor of the cancer microenvironment.

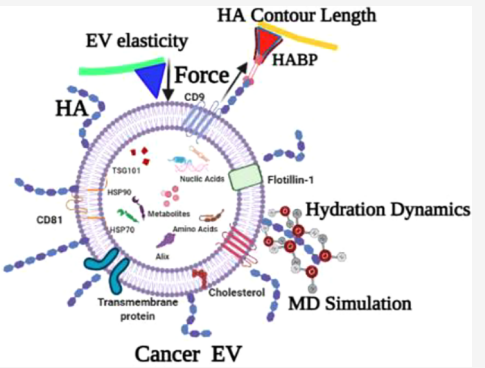

Extracellular vesicles (EVs) are lipid bilayer enclosed, nanosized pouches secreted from cells, carry unique biomolecules including proteins, nucleic acids, and carbohydrates on their surface or inside, and are imperative for cell signaling in multicellular organisms.[1−3] The three main subtypes of EVs are microvesicles (MVs), exosomes, and apoptotic bodies, depending on their biogenesis, content, release mechanism, size, and functions.[1,2] Recently, EVs have emerged as promising biomarkers of various cancers including colon cancer, the most prevalent malignancy of the human digestive system, and are undergoing clinical trials.[4] Recent findings suggest that hyaluronan (HA), a nonsulfated glycosaminoglycan, covers the cancer EV surface (HA-EVs) and is a potential biomarker for the early detection of colon cancer (Figure 1A).[5] In adenocarcinoma, upregulations of HA and CD44, an HA receptor protein, are directly implicated in metastasis.[6] Importantly, the length of HA controls its receptor sensitivity. HA carries danger signals in tumor progression when it gets fragmented by hyaluronidases (Hyals) and reactive oxygen species (ROS).[7] Therefore, there exists an unmet need of quantifying HA lengths attached to EVs that may be corroborated by the pathological state of the parent cells.

EVs experience multiple external forces during extracellular transportation, uptake, and excretion by cells, adhesion to cell surfaces, etc., which consequently modify their circulation time and also affect the release of biomolecules from EVs to cells or tissues. These forces temper the EV pliability, and therefore, EV elasticity measurements are pertinent to gain insight into the cancer microenvironment. In this work, we developed a strategy to measure the contour length of HA on an EV surface by single-molecule force spectroscopy (SMFS) exploiting the HA binding protein (HABP) interactions. Next, we ascertained the elasticity of single cancer EVs using atomic force microscopy (AFM) nanoindentation, compared the results with normal cell-derived EVs, and correlated the abundance of HA on the EVs to its intrinsic elasticity. We also explored the correlation between mechanical properties of EVs with abundance and length of HA fragments using solvation relaxation dynamics by fluorescence anisotropy and molecular dynamics (MD) simulations to support our claims.

Contour Length (Lc) of HA Polymers on EV Surface. In SMFS experiments, the interactions of binding cohorts, HA on the cancer EVs (colon HCT 116) immobilized on mica (as an EV film) and HABP (Figure 1A) covalently anchored to the AFM tip (Figure 1B), identified by their bond dissociation at a characteristic tip−substrate separation, are measured and fitted with worm-like chain (WLC) model, while fitting both persistence length (Lp) and the contour length (Lc) are set as adjustable parameters. For most of the curves the Lp agrees with values previously reported (4.1−4.4 nm) (Figure 1D,G) from single-molecule HA stretching experiments at comparable solution properties. Therefore, the data described here show

Received: June 1, 2022
Accepted: August 31, 2022
Published: September 7, 2022

https://doi.org/10.1021/acs.jpclett.2c01629
J. Phys. Chem. Lett. 2022, 13, 8564−8572

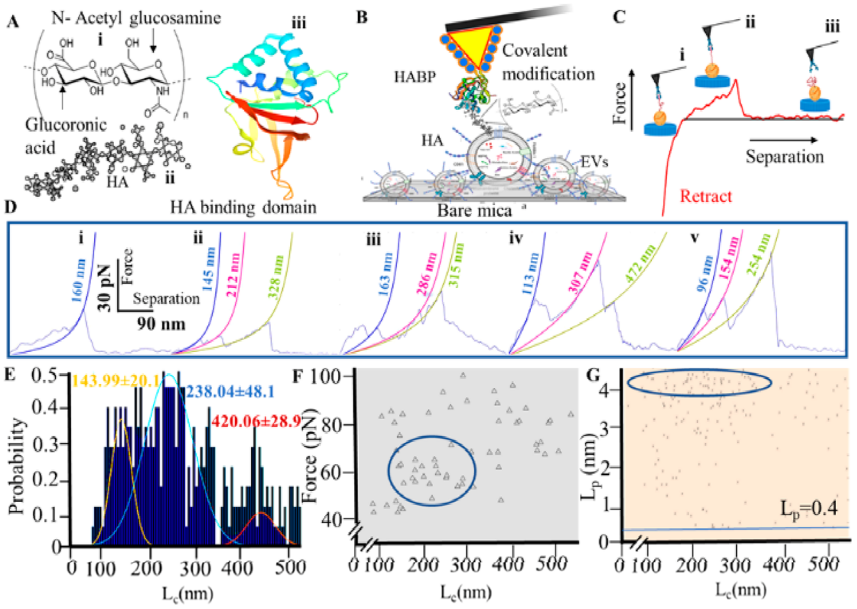

Figure 1. (A) Structure of HA, its molecular structure consists of two sugar molecules, glucuronic acid, and *N*-acetyl glucosamine (i), fully extended threefold helical structure of HA in ball-and-stick model, PDB ID: 1HYA (ii), crystal structure of HA binding domain, PDB ID: 5N86 (iii). (B) Model AFM pulling experiment having HA-EV film on mica at the bottom and AFM cantilever covalently modified with HABP approaching the surface and retracts while showing rupture events. (C) A typical retract curve showing the HA-HABP interaction, the parabolic area represents the binding and stretching of HA ((i)-(ii) -(iii)), the black line represents the baseline. (D) Sample retract curves for single (i) and multiple (ii)−(v) rupture events, corresponding L_cs are quantified by WLC fitting. (E) Multi-Gaussian fit (blue, red, and yellow lines) predicts the mean ± SD. L_c values of HA. (F) Unbinding force vs L_c values reflecting many data points around L_c = 200−240 nm (circled) with forces 50−60 pN. (G) L_p values of individual L_c measured, most of the curves fitted with WLC with L_p values 4.1−4.4 nm (circled). Two-dimensional probability distribution was performed with 1F and 1G data sets to check the statistical importance of the circled ranges (Supporting Information Figure S1).

the force−extension profile of a long, single/a few HA molecule(s) under stretching followed by a rupture event and provide the combined length of binding partners between the tip and substrate (L_c) (Figure 1C,D). The frequency of unbinding events is ∼70%, which points out that observed rupture forces are specific for HA and HABP interactions. Most of them showed multiple interaction signatures (Figure 1D(ii)−(v)); while only 5% represented a single unbinding event (Figure 1D(i)), the nonspecific interaction curves are carefully excluded. Interpretation of observed distributions of L_c fitted with multiple Gaussian functions (Figure 1E) relies on the simplest scenario, that each tethering end is placed face to face with each other (Figure 1B). In practice, interpretation of L_c is complicated by multiple factors, namely, (a) the presence of several HABP molecules immobilized on the AFM tip surface and the abundance of HA molecules on the HA-EV surface, which contributes to the measured unbinding force, (b) HABP location on the AFM tip relative to the EV on mica, and (c) HABP can bind at any position along the HA homopolymer chain,[8] giving rise to apparently different L_c values. For our system, the most probable L_c for HA is 238.0 ± 48.1 nm; the other two possible L_cs are 144.0 ± 20.1 and 420.0 ± 28.9 nm (Figure 1E). L_c is the simplest descriptor of polymer size defined as the length of the fully stretched polymer while disregarding the bond angles, unlike chain length, which is shorter than L_c. Now, L_c = 238 nm corresponds to ∼200−225 nm long HA with molecular weight (MW) 85−90 kDa,[9] where L_c of one disaccharide is 1 nm and MW is ∼0.38 kDa.[10] Similarly, for L_cs 143 and 420 nm, HA chain lengths are 120−140 and 390−410 nm with MWs 55−60 kDa and 155−160 kDa[9] respectively. Previous reports suggest that low molecular weight hyaluronan (LMW-HA) (<200 kDa) induces inflammation, which helps cancer to grow and metastasize, whereas high molecular weight hyaluronan (HMW-HA) (200−2000 kDa),[7] which prevails in normal conditions, is anti-inflammatory. HA production increases under inflammatory conditions by hyaluronan synthases, but, the produced HA also gets degraded by hyaluronidases (Hyals) and ROS to generate smaller HA fragments. Moreover, receptors (CD44, RHAMM, etc.) of HA are sensitive to the HA size.[7] Therefore, the HA fragment size could be a sensor of the state of the cancer progression not only surrounding the cell but also to distant organs due to circulating EVs. Now, sensitive and reproducible technologies for HA quantification and size determination in body fluid are not achieved yet. The EV samples collected from body fluids have intrinsic limitations, for example, sample amount, difficulty in purification, etc. Moreover, characterizing LMW-HA is technically challenging. Common possible techniques include enzyme-linked immunosorbent assay (ELISA), matrix-assisted laser desorption/ionization time-of-flight mass spectrometry (MALDI-TOF MS), or chromatography; most of them require a purified sample and calibration with purified multiple HA samples of known size (relatively expensive), and they also suffer from poor signal-to-background ratio and sensitivity issues. In this regard SMFS could be a viable alternative despite being time-intensive.

Mechanical Characteristics of HA-EVs. Next, we seek to quantify the elasticity of single EVs. AFM, in particular, has become a preferred technique for imaging EVs permitting nanoscale spatial resolution and piconewton-level force sensitivity for mechanical characterization under near-physiological conditions.[11] We visualized the scattered round-shaped EVs adsorbed on mica using tapping mode AFM; the typical

https://doi.org/10.1021/acs.jpclett.2c01629
J. Phys. Chem. Lett. 2022, 13, 8564−8572

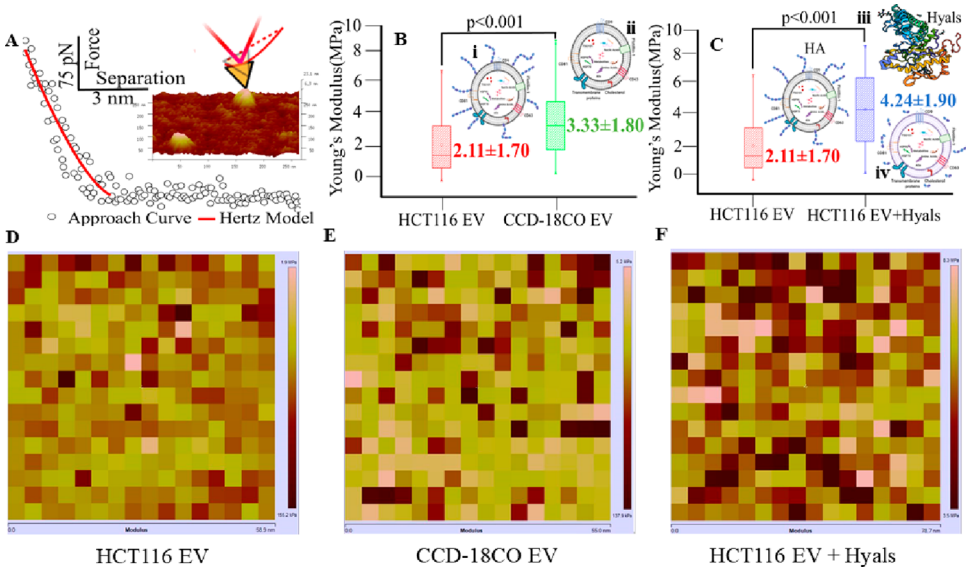

Figure 2. (A) A sample force−separation profile representing AFM nanoindentation on a single EV particle fitted with Hertz model with spherical indenter geometry, a 3D topographic view of scattered EVs on mica under buffer (inset). (B) Measured Young's modulus (E) values for HCT116 (cancer) and CCD-18CO (normal) EVs with respective mean ± SD. EV schematics showing HA molecules on HCT 116 EVs (i) and CCD-18CO EVs (ii). (C) Hyaluronidase (Hyals, PDB ID: 2PE4) catalyzes the degradation of HA (iii), E values before and after Hyals treatment on cancer EVs with respective mean ± SD. Schematic of Hyals treated HCT116 EVs (iv). The elasticity maps on single EV particles for HCT116 (D), CCD-18CO (E) and Hyals treated HCT116 EVs (F).

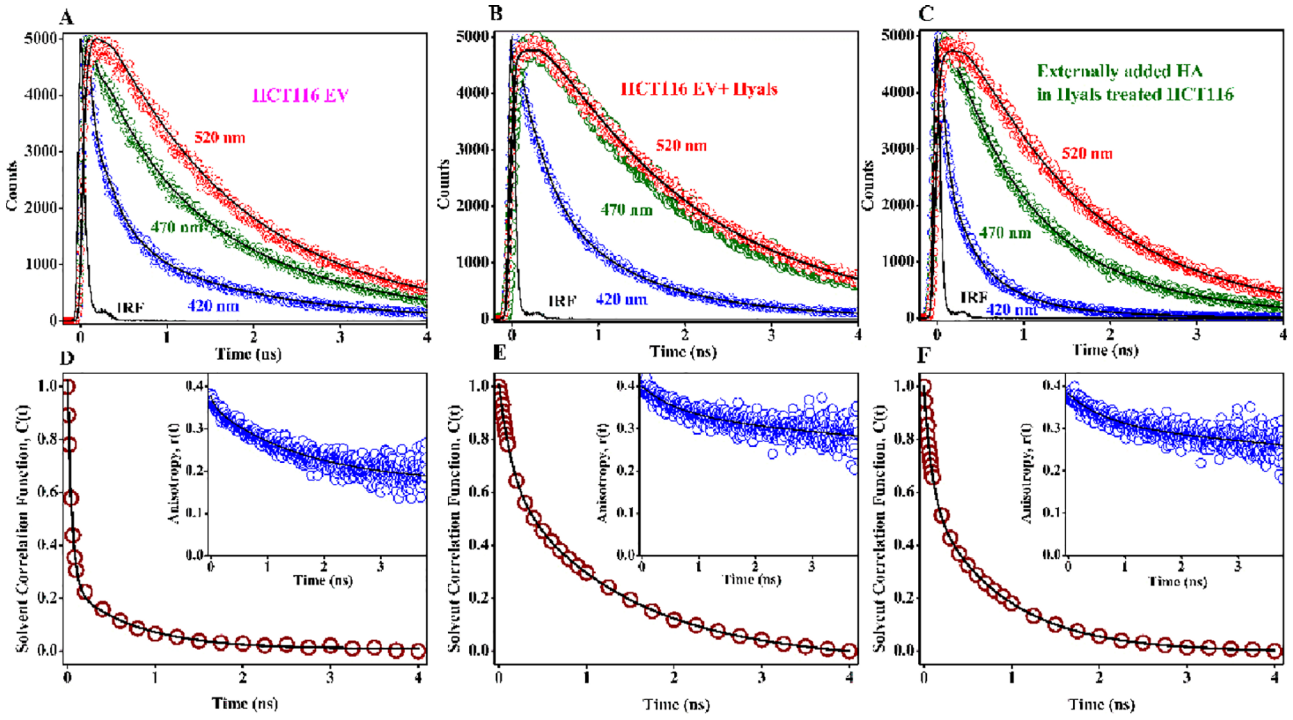

Figure 3. (A−C) Picosecond-resolved fluorescence transients of ACYMAN in HCT116 EVs, Hyals-treated EVs, and Hyals-treated EVs with added HA. Corresponding solvation correlation function of ACYMAN (D−F). Insets of D−F depict the fluorescence anisotropy of ACYMAN.

dimensions of HA-EVs are 49.5 ± 11.2 nm (diameter) and 20.7 ± 5.3 nm (height) under phosphate-buffered saline (PBS) buffer (Figure 2A, inset). AFM nanoindentation mode extracts a force−separation curve describing the force exerted (200−300 pN) on a single EV by the AFM tip as the tip indents the EV (it is not more than 3 nm; indentations are kept minimum to ensure noninvasive measurements) (Figure 2A). Young's modulus (E) is obtained by fitting the approach curve with the Hertz model (spherical indenter geometry). Interestingly, we revealed that the HA-EVs are significantly more elastic compared to the normal EVs (2.11 ± 1.70 vs 3.33 ± 1.80 MPa, $p < 0.001$) (Figure 2B,D,E), consistent with earlier reports.[12] This intrinsic resilience of cancer EVs indicate that elasticity has a profound influence on EV's biological role and potential biomarker functions.[13] This label-free analysis of individual EVs provides crucial insights into the biophysical

https://doi.org/10.1021/acs.jpclett.2c01629
J. Phys. Chem. Lett. 2022, 13, 8564−8572

distinctions among the EV populations having different pathological conditions. Next, we investigated the underlying factors that dictate this inherent elastic nature of cancer HA-EVs. We treated HA-EVs with Hyals to degrade the HA molecules (<200 kDa for our system). The HA degradation was validated by measuring Zeta potential (−19.2 ± 2.1 and −12.5 ± 1.2 mV before and after Hyals enzyme treatment, respectively) and Fourier transform infrared (FTIR) spectroscopy (Figure S6, Table S2).[5]

The elasticity values of the Hyals-treated EVs showed an appreciable increase from 2.11 ± 1.70 MPa (before treatment) to 4.24 ± 1.90 MPa ($p < 0.001$) (after treatment) (Figure 2C,D,F). Stiffness values of these EV samples also followed the same trend of elastic properties, cancer EVs (34.95 ± 8.95 pN/nm) > normal EVs (53.09 ± 9.28 pN/nm) > Hyals treated cancer EVs (60.30 ± 10.36 pN/nm) (Supporting Information Figure S2), consistent with the previous reports on soft samples.[14,15] These observations prove that accumulation of LMW-HA is directly correlated to the flexibility of HA-EVs. We also tried to visualize Hyals-treated EVs with externally added HMW-HA with AFM (to check if we could induce elasticity to the Hyals-treated EVs), but, unfortunately, we could not observe any discernible single EV on the surface.

It is reported that networks of negatively charged glycosaminoglycan HA polymers trap water and impede their movement,[16] which makes HA an ideal component of hydrogels, where HA content is correlated with the hydrogel viscosity and stiffness properties.[17] Similarly, increased HA content within tissues are known to cause swelling. We propose that the hydroscopic properties of LMW-HA employ and order water molecules on EV surroundings, thus acting as a cushion on the EV's outer surface and lowering the stiffness, which could be reinforced with shorter HA fragments since they are less viscous than HMW-HA. The HA receptors[18] and proteoglycans can also play critical roles in influencing HA-EV elasticity.

Photophysical Insights and Water Relaxation Dynamics. To gain more insight into the nature of the HA-associated water network and LMW-HA-induced flexibility/rigidity on the EV surface, we employed solvation relaxation of the water molecules and fluorescence anisotropy by using an interfacial fluorescent probe ACYMAN.[19−21] Figure 3 shows the wavelength-dependent fluorescence decays of ACYMAN (Scheme S1) in cancer EVs, Hyals-treated cancer EVs, and Hyals-treated EVs with externally added HA, respectively. The emission transients of (Figure 3A−C) ACYMAN on an EV surface are characterized by a decay in the blue end (420 nm) and a rise in the red end of the steady-state emission spectra, which is typical of solvent relaxation.[19] The relaxation of water molecules and associated EVs at the HA-EVs interface are manifested by a time-dependent Stokes shift of the fluorescence spectrum (TDFSS) to the red (Figure S3).

We then calculated the corresponding solvent correlation functions (Figure 3D−F). For cancer LMW-HA-EVs, the solvation correlation function $C(t)$ decays with two time constants 53 ps (81%) and 686 ps (19%) (Table 1),[22] which clearly indicated two types of water trajectories, which could be the contributions from LMW-HA-associated labile water molecules and water molecules present in the system (Scheme 1). We noticed a subtle but distinct difference in the solvation correlation function of water relaxation before and after Hyals treatment on the EVs (Table 1), the faster component of solvation ($\tau s1$) increased more than threefold, and a significant increase (19% to 72%) in the contribution of the slower component ($\tau s2$) is noticed. It is possible that the enzyme molecules on EV's surface induced a crowded environment, which poses significant restriction on the structural fluctuation of the EVs compared to LMW-HA-EVs. Next, we added HA molecules externally to the Hyals-treated EVs, which are possibly recognized by empty CD44 receptors (Figure 3F) (Figure S4). We also observed a notable change in the zeta potential value when we externally added HA into Hyals-treated EV sample (from −12.5 ± 1.2 to −14.95 ± 0.05 mV). Here, the time scale of the solvation correlation function was found to be quite similar (Table 1) to that of the LMW-HA-EVs. This could be linked to returning back to the same local environment around ACYMAN in the EV system. Next, to gain a better understanding of LMW-HA-induced flexibility/rigidity on HA-EVs, we performed fluorescence anisotropy.[23−29] The faster component ($\varphi 1$) (equation S1) was attributed to the local motion of the probe molecule (ACYMAN), whereas the longer nanosecond component ($\varphi 2$) carried the information regarding the segmental motion of the ACYMAN as it is inside the EVs. After Hyals treatment to the LMW-HA-EVs, time-resolved fluorescence anisotropy of ACYMAN on EVs (average rotational time scale, $\langle \tau r \rangle \approx 1910$ ps) became significantly retarded compared to that of the LMW-HA-EVs (average rotational time scale, $\langle \tau r \rangle \approx 1440$ ps) (Table 2) (insets of Figure 3) (Table S1).

These results suggested that the LMW-HA-associated labile water network is imparting flexibility to the EVs; upon Hyals treatment, this labile water network is disturbed, and the EV surfaces become hindered with the Hyals enzyme molecules. Next, we noticed that, upon external addition of HA on Hyals-treated EVs, the rotational relaxation time of ACYMAN became faster and comparable with LMW-HA-EVs, which therefore confirms the fact that HA induced a flexible environment on EVs' surface.

Molecular Dynamics Simulation. In experiments, the membranes surrounding the EVs are complex in terms of lipid composition and due to the presence of HA receptor proteins. Moreover the solvent dispersing the EVs consists of HA of different sizes and Hyals. We performed all-atom molecular dynamics simulations to qualitatively understand our experimental observations on elastic properties of a membrane in the presence of HA and relate them to the experimental findings. We considered a simple model of dipalmitoylphosphatidylcholine (DPPC) membrane. Although membrane composition is known to affect membrane properties and elasticity[30] PC lipids were chosen because of their upraised level in colon cancer cells compared to normal cells.[31] Due to an inherent limitation of computation power, we could consider HA chains much shorter than those in the

Table 1. Solvent Correlation Function of ACYMAN[a]

system	$\tau 1$/ns (%)	$\tau 2$/ns (%)	$\langle \tau \rangle$/ns (%)
HCT116	0.053 (81%)	0.686 (19%)	0.17
HCT116 + Hyals	0.168 (28%)	1.18 (72%)	0.89
HCT116 + Hyals + HA	0.107 (45%)	0.706 (55%)	0.43

[a]The excited-state relaxation dynamics of a fluorophore (τfast) may be acceptable up to the time scale of one-fifth of the instrument response function.[42,43] There are several articles from our group and other laboratories that also reported ∼50−70 ps of the relaxation time scale as one of the major components by using picosecond LASER of pulse width 70−80 ps.[44−48]

https://doi.org/10.1021/acs.jpclett.2c01629
J. Phys. Chem. Lett. 2022, 13, 8564−8572

Scheme 1[a]

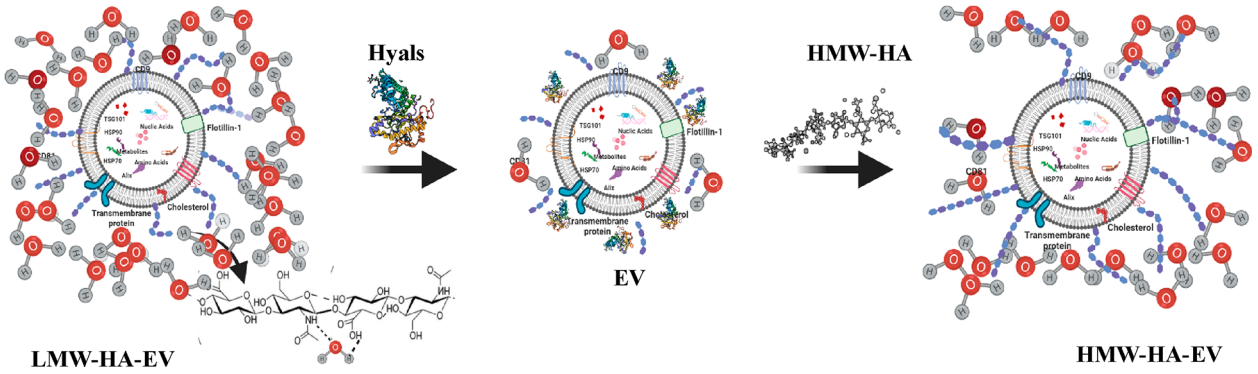

[a]In LMW-HA-EVs, the hygroscopic HA polymers are associated with a large number of water molecules on the EV surface. After Hyals treatment, HA molecules are degraded; therefore, in absence of HA, Hyals molecules could interact with the EV surface giving rise to a crowded environment. After HMW-HA addition, hygroscopic HA polymers are now again associated with water molecules. Bulk water solvation is not taken into account due to the very fast solvation of the bulk-type water molecules at the HA-water interface. Zewail et al. evaluated Trp solvation in bulk water with the solvation component 180 fs (78%) and 1.1 ps (22%), respectively, in a femtosecond fluorescence upconversion experiment. Furthermore, several fluorophores like 2-aminopurine, 1-anilinonaphthalene-8-sulfonate (ANS), andHoechst 33258 in bulk water show the two relaxation time components of 200 fs (15%) and 870 fs (85%) in the decay of solvation correlation function.[49] Please note, in our TCSPC set up, no rise component associated with bulk water relaxation could be detected with a time resolution of ∼20 ps.

Table 2. Rotational Relaxation Parameters of ACYMAN in the Following Three Samples[a]

system	τ/ns (%)	τ/ns (%)	τ/ns (%)
HCT116	0.080 (11%)	1.61 (89%)	1.44
HCT116 + Hyals	0.32 (23%)	2.39 (77%)	1.91
HCT116 + Hyals + HA	0.18 (46%)	1.68 (54%)	0.99

[a]The anisotropy decay of ACYMAN is characterized by two time constants with a much longer average rotational relaxation time (∼1440 ps) for cancer EVs relative to buffer (∼120 ps), which was consistent with the significantly hindered orientational motion of the probe in the rigid membrane of the extracellular vesicles compared to bulk water. Upon addition of Hyals on cancer EVs, the average rotational time constant increases significantly to ∼1910 ps relative to that of cancer EVs, indicating much slower orientational relaxation of the dye in the former than the latter. This is consistent with increased rigidity of the dye environment in the presence of Hyals by degrading the HA molecules on the EV surface.

experiments. We varied HA monomer numbers in the simulation box for a fixed chain length and HA chain length for a given monomer number.

The studies were carried out for a bilayer consisting of total 512 DPPC lipid molecules with 256 molecules in each monolayer. We considered 10, 30, and 50 HA pentamer (HA5), respectively (n_{HA5}= 10, 30, and 50), above the bilayer and HA molecules of different chain lengths: 150 HA monomer (HA1), 30 HA pentamer (HA5), and 15 HA decamer (HA10) with N = 1, 5, and 10, respectively (Figure S7). The equilibration of each system was ensured through the convergence of the area per lipid (APL) value of the DPPC bilayer with time (Figure S8).[32] We also calculated the time correlation function of the APL shown in the inset of Supporting Information Figure S8A−F. The correlation time scales are close to 1−2 ns for each system (see Supporting Information Table S3), similar to previous reports.[32] We divide the equilibrium trajectory into eight equal windows consisting snapshots of 50 ns. The time interval is sufficiently large to ensure the decay of APL correlation, and the blocks can be treated as independent ones to estimate mean and standard error of the mean of different quantities.

We calculated local density profiles of the constituent molecules of the system along the normal direction to the bilayer plane (z-axis in our case) with origin at the bilayer center. Supporting Information Figure S9A shows the density profile of phosphorus atoms $\rho_P(Z)$ of the DPPC bilayer, water molecules $\rho_W(Z)$, and HA $\rho_{HA}(Z)$ for different n_{HA5}. The peak observed in the $\rho_P(z)$ profile at a distance of 20 Å from the bilayer center indicates bilayer separation of about 40 Å, which is consistent with known bilayer thickness. $\rho_W(Z)$ vanishes at the bilayer center, as water does not enter the hydrophobic core of the membrane. It increases rapidly in the DPPC-water interfacial region between 20 Å and 30 Å and reaches bulk water density. $\rho_{HA}(z)$ shows peak at about 30 Å distance from the bilayer. The peak location indicates accumulation of HA molecules just outside the DPPC-water interface. Figure S9B shows the density profiles for different N. We note similar profiles as in Figure S9A. Moreover, the water density profile is found sensitive neither to HA concentration nor to HA aggregation state. Hence, the HA molecules interact with the lipid molecules indirectly via water molecules. We calculated the radial distribution function (rdf) of OW atoms of water around P atoms ($g_{P-OW}(r)$) for free and adsorbed lipids (shown in Figure S10), where r is the distance between P and OW atoms. $g_{P-OW}(r)$) remains the same for both cases across the systems. This implies that HA does not alter the hydration nature of the bilayer and, thus, emphasizes the importance of water-mediated interaction between HA and DPPC. The data are consistent with our experiments and earlier reports.[10]

Next, we calculated the area compressibility modulus ($k_A = k_BT$ ($\langle A\rangle/\langle\delta A^2\rangle$)) of the bilayer[32] from the equilibrium mean lateral area of the bilayer $\langle A\rangle$ and the fluctuations of lateral area of DPPC bilayer ($\langle\delta A^2\rangle = \langle(A - \langle A\rangle)^2\rangle$) for different systems. We find that $\langle A\rangle$ remains unaffected, as shown in Supporting Information Figure S11A. This leads us to consider $\langle\delta A^2\rangle$ in detail. All the data shown in Figure 4A−F are relative to respective quantities from pure DPPC simulation without any HA. In Figure 4A and its inset, we show the variation of

https://doi.org/10.1021/acs.jpclett.2c01629
J. Phys. Chem. Lett. 2022, 13, 8564−8572

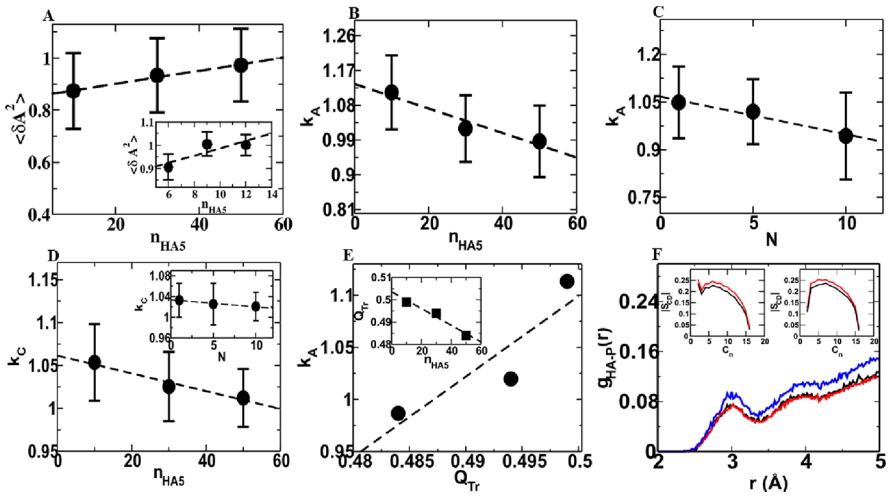

Figure 4. (A) Relative area fluctuation $\langle \delta A^2 \rangle$ for 512 DPPC bilayer and 128 DPPC bilayer (inset) with n_{HA5}. (B) Relative compressibility modulus k_A for different n_{HA5} and (C) for different N. (D) Relative bending modulus k_c for differentn_{HA5} and N (inset). (E) k_A vs tetrahedral order Q_{tr} of interfacial water molecules. (inset) Q_{tr} vs n_{HA5} plot. (F) RDF of P atoms of DPPC around heavy atoms of HA, $g_{HA-P}(r)$ for n_{HA5} = 10 (black), 30 (red), and 50 (blue). (insets) S_{CD} of sn1 (left panel) and sn2 (right panel) chain of free (black) and adsorbed lipids (red) for n_{HA5} = 50.

$\langle \delta A^2 \rangle$ with n_{HA5} of 512 DPPC and that of 128 DPPC bilayer, to check the system size dependence of this quantity. We find $\langle \delta A^2 \rangle$ increases linearly as n_{HA5} increases, and the trend is not sensitive to the system size. We find that the different quantities for systems with 128 DPPC follow the same trend in Supporting Information Figure S12 as in systems with 512 DPPC bilayers. This shows the convergence of our data with respect to the system size.

Since $\langle A \rangle$ is not sensitive to n_{HA5} or N, the dependence of k_A on n_{HA5} and N is dictated by the area fluctuation $\langle \delta A^2 \rangle$. Figure 4B shows variation of k_A with n_{HA5}. k_A decreases linearly with n_{HA5}. Figure 4C represents linear decrease of k_A with N, which is similar to the dependence in Figure 4B. The decrease in k_A with n_{HA5} and N indicates that the membrane shows enehanced elastic flexibility with n_{HA5} and N. We also calculate the bending modulus (k_C) of the DPPC bilayer for different cases from the equilibrium height fluctuation of the bilayer (details are in Methods).[33] Figure 4D shows relative bending modulus k_c versus n_{HA5}, and k_c versus N data are shown in the inset of Figure 4D. We find k_c decreases with increase in both n_{HA} and N within the error bars. The qualitative trends are similar to those of k_A. Thus, k_A and k_C of a DPPC lipid bilayer decrease with increase in both n_{HA5} and N, suggesting softening of the bilayer. This is qualitatively similar to the experimental observations. The effects of n_{HA5} appears to be stronger than those of N.

Since HA interaction with the bilayer is mediated via water, we examine how the interfacial water molecules respond to the changes in n_{HA5} in order to understand the microscopic origin of the elastic response. We consider the changes in the tetrahedral order parameter Q_{tr} of the water molecules in the interface extending up to z = 15 Å above the average z position of phosphorus atom.[34] The average z position of phosphorus is taken by the peaks of $\rho_p(z)$. We note that the Q_{tr} decreases as n_{HA5} increases (inset of Figure 4E). The water molecules tend to hydrate HA molecules here. They get slightly disordered due to the random orientation of HA pentamers (see the snapshot in Supporting Information Figure S7). Figure 4E describes the variation of k_A with Q_{tr}. We find that k_A increases as Q_{tr} increases. Thus, the disorder in the tetrahedral network makes the membrane fluctuate more. We further probe the mechanistic picture leading to this behavior. To this end we calculated the rdf of P atoms around the heavy atoms of HA ($g_{HA-P}(r)$), where r is the distance between P and any heavy atoms of HA. The data in Figure 4F show the first peak around r = 3 Å, and the peak height increases with n_{HA5}. This behavior along with that of Q_{tr} suggests that the disorder in the tetrahedral network of water helps the HA to approach the P atoms better. Next we calculated the order parameter of acyl chains (S_{CD}) for both free lipids and those having HA in the vicinity (calculation details are in Methods). S_{CD} for sn1 and sn2 chains of both lipids species for n_{HA5} = 50 are shown in the insets of Figure 4F, while other cases are shown in Supporting Information Figure S13. We found an increase in S_{CD} when HA is adsorbed to the DPPC molecules, suggesting enhancement of order in lipid tails. Both the mean thickness of the membrane (d_{P-P}) and the roughness, given by the root-mean-square deviation (RMSD) of the z coordinates of the adsorbed lipids, increase with increasing n_{HA5} as shown in Supporting Information Figure S14. Thus, the ordering of the tails enhances registry between successive lipid molecules facilitating both out-of-plane and lateral movements so that the area per lipid shows more fluctuations.

Our AFM experiments show that the rigidity decreases for HA-coated cancer EVs (HA abundance) in comparison to normal EVs, and the photophysical hydration dynamics data imply that, with HA added externally onto Hyals-treated EVs, a flexible environment is induced around the EVs. These two experimental results are consistent with the dependence of k_A with n_{HA5}. Experimentally we further observe that the EV membrane becomes less flexible by adding hyaluronidase, which promotes HA degradation. This is consistent qualitatively with the decrease of k_A with increasing N obsreved in the simulations. It may be noted that, in bilayer systems, polar and hydrophilic ligands like TAT polypeptide,[35] glyphosphate,[36] polycation,[37] hydronium ions,[38] and diols[39]

https://doi.org/10.1021/acs.jpclett.2c01629
J. Phys. Chem. Lett. 2022, 13, 8564−8572

stay in the vicinity of the headgroups, while hydrophobic ligands like polystyrene[40] or amphipathic ligands like quercetin[41] penetrate into the membrane. In such cases the bilayer shows substantial deformation and changes in elastic properties. However, the water-mediated elastic response of the bilayer without a prominent structural deformation in the presence of HA has not been reported so far to the best of our knowledge. Therefore, our primary experimental observations on the elastic response of the EV membrane induced by HA can be understood in the light of water-mediated interaction between HA and bilayers.

We also tested the direct implication of the elasticity of the HA-EVs with its biological function. We combined doxorubicin, a positively charged chemotherapeutic drug, with HA-EVs, HA-EVs treated with Hyals, and normal cell EVs. Our results clearly revealed that HA-EVs were preferentially taken by the cancer cells (HCT 116 and MCF 7, Supporting Information Figures S15–S17) than the HA-depleted EVs or normal cell EVs. Therefore, the intrinsic elastic nature of HA-EVs is indeed playing a crucial role in enhancing its cellular uptake efficiency.

Collectively, we conclude that cancer cell-derived HA-EVs are special vehicles for LMW-HA (<200 kDa), significantly more flexible than the normal EVs due to HA profusion, carry unique signals important for malignant growth, and offer a novel link between the mechanical properties of HA and cancer malignancy. Henceforth, the distinct mechanoelastic behavior of HA-EVs is a promising biosensor in the study of cancer.

■ ASSOCIATED CONTENT

Supporting Information

The Supporting Information is available free of charge at https://pubs.acs.org/doi/10.1021/acs.jpclett.2c01629.

Experimental methods include details of cell culture, EV isolation, Zeta potential, FT-IR, AFM imaging, SMFS including unbinding and elasticity measurements, photophysical experiments, and molecular dynamics simulation details (PDF)

Transparent Peer Review report available (PDF)

■ AUTHOR INFORMATION

Corresponding Authors

Suchetan Pal − *Department of Chemistry, Indian Institute of Technology, Bhilai CG 492015, India*; Email: suchetanp@iitbhilai.ac.in

Dulal Senapati − *Chemical Science Division, Saha Institute of Nuclear Physics, Kolkata 700064, India*; orcid.org/0000-0001-5002-4631; Email: dulal.senapati@saha.ac.in

Jaydeb Chakrabarti − *Department of Physics of Complex Systems, S. N. Bose National Centre for Basic Sciences, Kolkata 700106, India; Department of Chemical and Biological Sciences, S. N. Bose National Centre for Basic Sciences, Kolkata 700106, India*; Email: jaydeb@bose.res.in

Samir Kumar Pal − *Department of Chemical and Biological Sciences, S. N. Bose National Centre for Basic Sciences, Kolkata 700106, India*; orcid.org/0000-0001-6943-5828; Email: skpal@bose.res.in

Tatini Rakshit − *Department of Chemistry, Shiv Nadar Institute of Eminence, Tehsil Dadri UP 201314 Uttar Pradesh, India*; orcid.org/0000-0002-4182-9240; Email: tatini.rakshit@snu.edu.in

Authors

Debashish Paul − *Department of Chemistry, Shiv Nadar Institute of Eminence, Tehsil Dadri UP 201314 Uttar Pradesh, India*; orcid.org/0000-0002-6764-5052

Anirban Paul − *Department of Physics of Complex Systems, S. N. Bose National Centre for Basic Sciences, Kolkata 700106, India*

Dipanjan Mukherjee − *Department of Chemical and Biological Sciences, S. N. Bose National Centre for Basic Sciences, Kolkata 700106, India*

Saroj Saroj − *Department of Chemistry, Shiv Nadar Institute of Eminence, Tehsil Dadri UP 201314 Uttar Pradesh, India*

Manorama Ghosal − *Chemical Science Division, Saha Institute of Nuclear Physics, Kolkata 700064, India*

Complete contact information is available at: https://pubs.acs.org/10.1021/acs.jpclett.2c01629

Author Contributions

#Equal contribution.

Notes

The authors declare no competing financial interest.

■ ACKNOWLEDGMENTS

D.P. and A.P. thank SERB-CRG and CSIR for JRF and SRF. We are thankful to Profs. R. Das and. S. Singha for providing the fluorescence dye. A.P. thanks Thematic Unit of Excellence and Technical Research Centre at SNBNCBS for computational facilities. S.P. thanks SERB (SRG/2019/000953) for funding. T.R. thanks SERB [CRG/2019/007013], [DST/INSPIRE/04/2017/002375], and Shiv Nadar IoE, Delhi-NCR, for generous funding and research facilities.

■ REFERENCES

(1) Kalluri, R.; LeBleu, V. S. The Biology, Function, and Biomedical Applications of Exosomes. *Science (80-.)* **2020**, *367* (640), 1–15.

(2) Datta, B.; Paul, D.; Pal, U.; Rakshit, T. Intriguing Biomedical Applications of Synthetic and Natural Cell-Derived Vesicles: A Comparative Overview. *ACS Appl. Bio Mater.* **2021**, *4* (4), 2863–2885.

(3) Datta, B.; Paul, D.; Dey, T.; Pal, S.; Rakshit, T. Importance of Extracellular Vesicle Derived RNAs as Critical Colorectal Cancer Biomarkers. *ACS Bio Med. Chem. Au* **2022**, *2* (3), 222–235.

(4) Piccinelli, M. The Atride Case. *Psicoter. e Sci. Um.* **2020**, *54* (3), 481–489.

(5) Paul, D.; Roy, A.; Nandy, A.; Datta, B.; Borar, P.; Pal, S. K.; Senapati, D.; Rakshit, T. Identification of Biomarker Hyaluronan on Colon Cancer Extracellular Vesicles Using Correlative AFM and Spectroscopy. *J. Phys. Chem. Lett.* **2020**, *11* (14), 5569–5576.

(6) Rilla, K.; Siiskonen, H.; Tammi, M.; Tammi, R. *Hyaluronan-Coated Extracellular Vesicles- A Novel Link between Hyaluronan and Cancer* **2014**, *123*, 121–148, DOI: 10.1016/B978-0-12-800092-2.00005-8.

(7) Cowman, M. K.; Lee, H. G.; Schwertfeger, K. L.; McCarthy, J. B.; Turley, E. A. The Content and Size of Hyaluronan in Biological Fluids and Tissues. *Front. Immunol.* **2015**, *6* (JUN), 1–8.

(8) Bano, F.; Tammi, M. I.; Kang, D. W.; Harris, E. N.; Richter, R. P. Single-Molecule Unbinding Forces between the Polysaccharide Hyaluronan and Its Binding Proteins. *Biophys. J.* **2018**, *114* (12), 2910–2922.

(9) Coleman, P. J.; Scott, D.; Mason, R. M.; Levick, J. R. Role of Hyaluronan Chain Length in Buffering Interstitial Flow across Synovium in Rabbits. *J. Physiol.* **2000**, *526* (2), 425–434.

(10) Smith, P.; Ziolek, R. M.; Gazzarrini, E.; Owen, D. M.; Lorenz, C. D. On the Interaction of Hyaluronic Acid with Synovial Fluid Lipid Membranes. *Phys. Chem. Chem. Phys.* **2019**, *21* (19), 9845–9857.

(11) Théry, C.; Witwer, K. W.; Aikawa, E.; Alcaraz, M. J.; Anderson, J. D.; Andriantsitohaina, R.; Antoniou, A.; Arab, T.; Archer, F.; Atkin-Smith, G. K.; et al. Minimal Information for Studies of Extracellular Vesicles 2018 (MISEV2018): A Position Statement of the International Society for Extracellular Vesicles and Update of the MISEV2014 Guidelines. *J. Extracell. Vesicles* **2018**, *7* (1), 1−43.
(12) LeClaire, M.; Gimzewski, J.; Sharma, S. A Review of the Biomechanical Properties of Single Extracellular Vesicles. *Nano Sel* **2021**, *2* (1), 1−15.
(13) Whitehead, B.; Wu, L. P.; Hvam, M. L.; Aslan, H.; Dong, M.; DyrskjØt, L.; Ostenfeld, M. S.; Moghimi, S. M.; Howard, K. A. Tumour Exosomes Display Differential Mechanical and Complement Activation Properties Dependent on Malignant State: Implications in Endothelial Leakiness. *J. Extracell. Vesicles* **2015**, *4* (1), 1−11.
(14) Mukherjee, D.; Rakshit, T.; Singh, P.; Mondal, S.; Paul, D.; Ahir, M.; Adhikari, A.; Puthiyapurayil, T. P.; Vemula, P. K.; Senapati, D.; Das, R.; Pal, S. K. Differential Flexibility Leading to Crucial Microelastic Properties of Asymmetric Lipid Vesicles for Cellular Transfection: A Combined Spectroscopic and Atomic Force Microscopy Studies. *Colloids Surfaces B Biointerfaces* **2020**, *196* (July), 1−10.
(15) Nandi, S.; Layek, S.; Nandi, P. K.; Bera, N.; Hazra, R.; Sarkar, N. Self-Assembled Etiologies of the Artificial Sweetener Aspartame Adversely Affect Phospholipid Membranes: A Plausible Reason for Its Deleterious Intake. *Chem. Commun.* **2021**, *57* (81), 10532−10535.
(16) Cowman, M. K.; Matsuoka, S. Experimental Approaches to Hyaluronan Structure. *Carbohydr. Res.* **2005**, *340* (5), 791−809.
(17) Serban, M. A.; Scott, A.; Prestwich, G. D. Use of Hyaluronan-Derived Hydrogels for Three-Dimensional Cell Culture and Tumor Xenografts. *Curr. Protoc. Cell Biol.* **2008**, *40*, 1−21.
(18) Misra, S.; Hascall, V. C.; Markwald, R. R.; Ghatak, S. Interactions between Hyaluronan and Its Receptors (CD44, RHAMM) Regulate the Activities of Inflammation and Cancer. *Front. Immunol.* **2015**, *6* (May), 1−31.
(19) Singh, P.; Choudhury, S.; Singha, S.; Jun, Y.; Chakraborty, S.; Sengupta, J.; Das, R.; Ahn, K. H.; Pal, S. K. A Sensitive Fluorescent Probe for the Polar Solvation Dynamics at Protein-Surfactant Interfaces. *Phys. Chem. Chem. Phys.* **2017**, *19* (19), 12237−12245.
(20) Singh, P.; Sharma, V. K.; Singha, S.; García Sakai, V.; Mukhopadhyay, R.; Das, R.; Pal, S. K. Unraveling the Role of Monoolein in Fluidity and Dynamical Response of a Mixed Cationic Lipid Bilayer. *Langmuir* **2019**, *35* (13), 4682−4692.
(21) Singh, P.; Mukherjee, D.; Singha, S.; Sharma, V. K.; Althagafi, I. I.; Ahmed, S. A.; Mukhopadhyay, R.; Das, R.; Pal, S. K. Probing Relaxation Dynamics of a Cationic Lipid Based Non-Viral Carrier: A Time-Resolved Fluorescence Study. *RSC Adv.* **2019**, *9* (61), 35549−35558.
(22) Ghosh, C.; Nandi, S.; Bhattacharyya, K. Probing Micro-Environment of Lipid Droplets in a Live Breast Cell: MCF7 and MCF10A. *Chem. Phys. Lett.* **2017**, *670*, 27−31.
(23) Kinosita, K.; Ikegami, A.; Kawato, S. On the Wobbling-in-Cone Analysis of Fluorescence Anisotropy Decay. *Biophys. J.* **1982**, *37* (2), 461−464.
(24) Mukherjee, D.; Singh, P.; Rakshit, T.; Puthiya-Purayil, T. P.; Vemula, P. K.; Sengupta, J.; Das, R.; Pal, S. K. Deciphering the Response of Asymmetry in the Hydrophobic Chains of Novel Cationic Lipids towards Biological Function. *Phys. Chem. Chem. Phys.* **2020**, *22* (3), 1738−1746.
(25) Mukherjee, D.; Paul, D.; Sarker, S.; Hasan, M. N.; Ghosh, R.; Prasad, S. E.; Vemula, P. K.; Das, R.; Adhikary, A.; Pal, S. K.; Rakshit, T. Polyethylene Glycol-Mediated Fusion of Extracellular Vesicles with Cationic Liposomes for the Design of Hybrid Delivery Systems. *ACS Appl. Bio Mater.* **2021**, *4* (12), 8259−8266.
(26) Nandi, S.; Pyne, A.; Layek, S.; Arora, C.; Sarkar, N. The Dietary Nutrient Trimethylamine N-Oxide Affects the Phospholipid Vesicle Membrane: Probable Route to Adverse Intake. *J. Phys. Chem. Lett.* **2021**, *12* (51), 12411−12418.
(27) Nandi, S.; Pyne, A.; Ghosh, M.; Banerjee, P.; Ghosh, B.; Sarkar, N. Antagonist Effects of l -Phenylalanine and the Enantiomeric Mixture Containing d -Phenylalanine on Phospholipid Vesicle Membrane. *Langmuir* **2020**, *36* (9), 2459−2473.
(28) Nandi, S.; Kundu, S.; Pyne, A.; Sarkar, N. Spectroscopic Investigation on Alteration of Dynamic Properties of Lipid Membrane in Presence of Gamma-Aminobutyric Acid (GABA). *J. Mol. Liq.* **2020**, *297*, 1−10.
(29) Nandi, S.; Mukhopadhyay, A.; Nandi, P. K.; Bera, N.; Hazra, R.; Chatterjee, J.; Sarkar, N. Amyloids Formed by Nonaromatic Amino Acid Methionine and Its Cross with Phenylalanine Significantly Affects Phospholipid Vesicle Membrane: An Insight into Hypermethioninemia Disorder. *Langmuir* **2022**, *38* (27), 8252−8265.
(30) Nguyen, H. L.; Man, V. H.; Li, M. S.; Derreumaux, P.; Wang, J.; Nguyen, P. H. Elastic Moduli of Normal and Cancer Cell Membranes Revealed by Molecular Dynamics Simulations. *Phys. Chem. Chem. Phys.* **2022**, *24* (10), 6225−6237.
(31) Khuntawee, W.; Amornloetwattana, R.; Vongsangnak, W.; Namdee, K.; Yata, T.; Karttunen, M.; Wong-Ekkabut, J. In Silicoandin Vitrodesign of Cordycepin Encapsulation in Liposomes for Colon Cancer Treatment. *RSC Adv.* **2021**, *11* (15), 8475−8484.
(32) Venable, R. M.; Brown, F. L. H.; Pastor, R. W. Mechanical Properties of Lipid Bilayers from Molecular Dynamics Simulation. *Chem. Phys. Lipids* **2015**, *192*, 60−74.
(33) Fowler, P. W.; Hélie, J.; Duncan, A.; Chavent, M.; Koldsø, H.; Sansom, M. S. P. Membrane Stiffness Is Modified by Integral Membrane Proteins. *Soft Matter* **2016**, *12* (37), 7792−7803.
(34) Chau, P.; Hardwick, A. J. A New Order Parameter for Tetrahedral Configurations. *Mol. Phys.* **1998**, *93* (3), 511−518.
(35) Patra, P.; Banerjee, R.; Chakrabarti, J. Effect of Biphosphate Salt on Dipalmitoylphosphatidylcholine Bilayer Deformation by Tat Polypeptide. *Biopolymers* **2022**, e23518, 1−11. .
(36) Frigini, E. N.; López Cascales, J. J.; Porasso, R. D. Molecular Dynamics Simulations of Glyphosate in a DPPC Lipid Bilayer. *Chem. Phys. Lipids* **2018**, *213*, 111−117.
(37) Kopec, W.; Zak, A.; Jamroz, D.; Nakahata, R.; Yusa, S. I.; Gapsys, V.; Kepczynski, M. Polycation-Anionic Lipid Membrane Interactions. *Langmuir* **2020**, *36* (42), 12435−12450.
(38) Deplazes, E.; Poger, D.; Cornell, B.; Cranfield, C. G. The Effect of Hydronium Ions on the Structure of Phospholipid Membranes. *Phys. Chem. Chem. Phys.* **2018**, *20* (1), 357−366.
(39) Rhys, N. H.; Barlow, D. J.; Lawrence, M. J.; Lorenz, C. D. On the Interactions of Diols and DMPC Monolayers. *J. Mol. Liq.* **2022**, *364*, 1−10.
(40) Bochicchio, D.; Cantu, L.; Cadario, M. V.; Palchetti, L.; Natali, F.; Monticelli, L.; Rossi, G.; Del Favero, E. Polystyrene Perturbs the Structure, Dynamics, and Mechanical Properties of DPPC Membranes: An Experimental and Computational Study. *J. Colloid Interface Sci.* **2022**, *605*, 110−119.
(41) Eid, J.; Jraij, A.; Greige-Gerges, H.; Monticelli, L. Effect of Quercetin on Lipid Membrane Rigidity: Assessment by Atomic Force Microscopy and Molecular Dynamics Simulations. *BBA Adv.* **2021**, *1* (June), 1−10.
(42) Connor, D. V. O. Time-Correlated Single Photon Counting. *Compendium of Chemical Terminology;* Blackwell Scientific Publications, 2008. DOI: 10.1351/goldbook.t06377.
(43) Becker, W. The Bh TCSPC Handbook. *Scanning* **2010**, *800*, 1−566.
(44) Sahu, K.; Mondal, S. K.; Roy, D.; Karmakar, R.; Bhattacharyya, K. Slow Solvation Dynamics of 4-AP and DCM in Binary Mixtures. *J. Photochem. Photobiol. A Chem.* **2005**, *172* (2), 180−184.
(45) Verma, P. K.; Mitra, R. K.; Pal, S. K. A Molecular Picture of Diffusion Controlled Reaction: Role of Microviscosity and Hydration on Hydrolysis of Benzoyl Chloride at a Polymer Hydration Region. *Langmuir* **2009**, *25* (19), 11336−11343.
(46) Rakshit, S.; Saha, R.; Verma, P. K.; Pal, S. K. Role of Solvation Dynamics in Excited State Proton Transfer of 1-Naphthol in Nanoscopic Water Clusters Formed in a Hydrophobic Solvent. *Photochem. Photobiol.* **2012**, *88* (4), 851−859.

(47) Banerjee, D.; Pal, S. K. Solvation Dynamics of LDS 750 in Micelles, Reverse Micelles and Proteins. *Chem. Phys. Lett.* **2008**, *451* (4−6), 237−242.
(48) Sarkar, R.; Ghosh, M.; Pal, S. K. Ultrafast Relaxation Dynamics of a Biologically Relevant Probe Dansyl at the Micellar Surface. *J. Photochem. Photobiol. B Biol.* **2005**, *78* (2), 93−98.
(49) Pal, S. K.; Zewail, A. H. Dynamics of Water in Biological Recognition. *Chem. Rev.* **2004**, *104* (4), 2099−2123.

https://doi.org/10.1021/acs.jpclett.2c01629
J. Phys. Chem. Lett. 2022, 13, 8564−8572